Green Chemistry

PAPER

Cite this: *Green Chem.*, 2020, **22**, 230

Biomimetic photocatalytic sulfonation of alkenes to access β-ketosulfones with single-atom iron site†

Jiangwei Wen,‡[a] Xiaoting Yang,‡[a] Zongzhao Sun,‡[b] Jianjing Yang,*[a] Ping Han,[a] Qiuxia Liu,[a] Hongyan Dong,[a] Meng Gu,[c] Limin Huang*[b] and Hua Wang *[a]

Received 16th October 2019,
Accepted 14th November 2019

DOI: 10.1039/c9gc03580j

rsc.li/greenchem

Biomimetic photocatalysis as an important organic transformation strategy has received increasing attention, with the performances of biomimetic catalysts largely depending on their design. This protocol has been initially used to fabricate a biomimetic photocatalyst of single-atom iron site through coupling carbon nitride with hemin (CNH) for the visible light-promoted sulfonation of alkenes to produce β-ketosulfones with up to 94% yield. The experimental results show that the role of CN in CNH is concentrated on enhancing the separation ability of photogenerated electron pairs and holes to improve the photocatalytic activity and stability. Moreover, the as-prepared photocatalyst of single atom iron can be irradiated under near-infrared light with a satisfactory yield, and is also feasible for the sulfonation reactions of androstenones. Importantly, this biomimetic catalysis-based synthesis system has some merits, namely high catalysis efficiency, favorable recyclability, high turnover number, and excellent functional group tolerance, making it promising for extensive applications in organic transformations for the synthesis of β-ketosulfones to access various bioactive drugs.

Introduction

Over the last few decades, homogeneous photoredox catalysis under visible light using metal complexes or organic dyes as sensitizers has become a powerful tool for the development of valuable transformations in organic synthesis.[1] However, homogeneous catalysis may have some intrinsic challenges such as high cost, non-recyclable catalysts, and harsh reaction conditions. To overcome these limitations, the development of visible light-induced heterogeneous catalysts has received great attention from chemists.[2] In particular, various kinds of heterogeneous photoredox catalysts have been successfully fabricated for a variety of organic transformations, such as semiconductors,[3] magnetic nanomaterials,[4] metal–organic frameworks (MOFs),[5] covalent organic frameworks (COFs),[6] polymeric graphitic carbon nitrides (CN)[2d,e,g,7] and noble metal-supported metal oxides.[2h,8] Nevertheless, the heterogeneous catalysis system, especially with a biomimetic single-atom-site catalyst under visible light, has rarely been reported for organic transformations with high efficiency in constructing highly bioactive drug blocks.[9]

β-Ketosulfones, as an important class of sulfone-containing organic molecules, have been widely used in the synthesis of a series of organic functional materials and pharmaceuticals.[10] Particularly, β-ketosulfones have recently attracted considerable synthetic attention due to their interesting biological activities[10d–g] and important synthetic applications[10h] (Fig. 1). Consequently, substantial efforts have been devoted to disco-

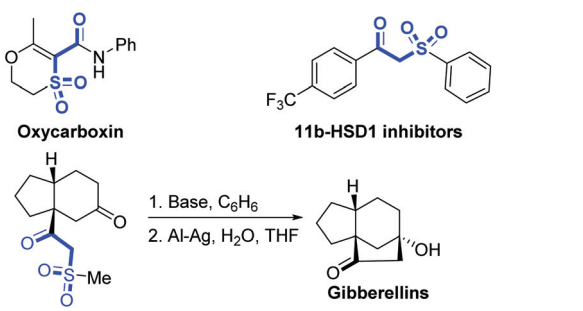

Fig. 1 Representative of β-ketosulfone-based bioactive molecules and synthetic applications.

[a]*Institute of Medicine and Materials Applied Technologies, College of Chemistry and Chemical Engineering, Qufu Normal University, Qufu, Shandong 273165, P. R. China. E-mail: huawang@qfnu.edu.cn*
[b]*Department of Chemistry, Southern University of Science and Technology, Shenzhen, Guangdong, 518055, China*
[c]*Department of Materials Science and Engineering, Southern University of Science and Technology, Shenzhen, Guangdong, 518055, China*

†Electronic supplementary information (ESI) available: Experimental procedure, characterization data, and copies of NMR spectra. See DOI: 10.1039/c9gc03580j

‡These authors contributed equally to this work.

vering efficient synthesis and functionalization strategies of β-ketosulfones.[11] Particularly, a variety of homogenous catalytic methods have been recently developed based on the sulfonation of alkenes to access β-ketosulfones. For example, Yadav and co-workers have proposed a highly efficient synthetic approach to access β-ketosulfones *via* the $AgNO_3/K_2S_2O_8$-catalyzed oxysulfonylation of alkenes with thiophenols or arenesulfinate salts.[11c,f] Our group has separately utilized $Cu(OAc)_2$, $FeCl_2$, and eosin-Y/TBHP as catalysts for the synthesis of β-ketosulfones starting from some terminal alkenes.[11b,e,g] In spite of several achievements made so far, the homogeneous nature of these catalytic transition metals and dyes is largely challenged by some limitations such as the unrecoverable catalyst, narrow absorption range and poor substrate scope (Fig. 2A). Therefore, it is highly desirable to develop more efficient, recyclable, and environmentally benign catalysts for heterogeneous photocatalysis reactions to access β-ketosulfones.

Recent decades have witnessed the increasing applications of metalloporphyrin-based biomimetic catalysis routes for the synthesis of numerous fine chemicals, such as alcohols, aldehydes, ketones, acids, esters, epoxies, sulfoxides, and imines because they are environmentally friendly, require low energy and operate under mild reaction conditions.[12] However, a vital challenge involves the design of biomimetic catalysts with high efficiency and especially visible light catalysis. In the present work, a biomimetic photocatalyst of single-atom iron site supported on carbon nitride has been designed for the first time simply by using a chemical coupling method, where the carboxyl groups of hemin were covalently attached to the terminal amino of CN, and it could be applied to the visible light-promoted sulfonation of alkenes to access β-ketosulfones with high efficiency (Fig. 2B). Importantly, the as-prepared photocatalyst containing single-atom iron site can be used even under near-infrared light irradiation, and is also generally used for the sulfonation reactions of androstenones. In terms of substrate scope, various alkenes and sulfinic acids or their salts are compatible with the present protocol, generating the desired products in up to 94% yields. It is worth noting that the visible light-promoted biomimetic catalytic sulfonation of alkenes can be used to access β-ketosulfones with a high turnover number (TON: up to 2861) and excellent recyclability.

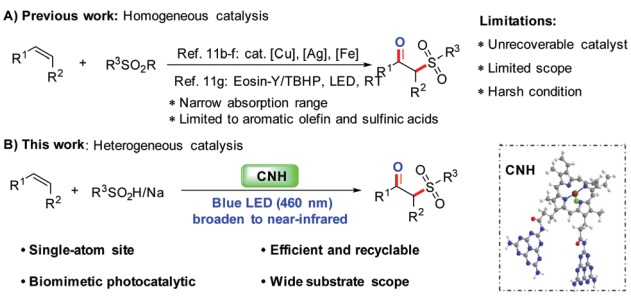

Fig. 2 Advantages of the biomimetic photocatalytic olefin sulfonation.

Results and discussion

Synthesis of carbon nitride-hemin (CNH) photocatalysts

A simple molecule coupling strategy was applied here to prepare CNH (Fig. 3). Briefly, carbon nitride was first fabricated by thermal decomposition of urea at 550 °C for 2 h in static air with a ramp rate of 5 °C min^{-1}, wherein the CN product could possess abundant functional $-NH_2$ groups (Fig. S1a†). Subsequently, following the concept of biomimetic catalysis, CNH was prepared by 1-(3-dimethylaminopropyl)-3-ethylcarbodiimide hydrochloride (EDC) and *N*-hydroxysuccinimide (NHS)-mediated molecular crosslinking of CN with hemin, as vividly shown in Fig. 3.

Morphological and structural characterization

The morphological and structural characterization of single-atom iron site-containing photoredox catalysts of CNH was carried out separately by FT-IR and UV spectroscopy, Brunauer–Emmett–Teller (BET) analysis, scanning electron microscopy (SEM) and high-angle annular dark-field scanning electron microscopy (HAADF-STEM) (Fig. S1† and Fig. 4). First and foremost, the FT-IR spectra of the dried CNH samples were recorded to investigate the appropriate functional groups during various formation stages of the photocatalysts. As can be seen from Fig. S1a,† after the chemical cross-linking of CN and hemin to yield CNH, the N–H absorption peak is significantly reduced, and three new peaks are observed at 1683 cm^{-1}, 1718 cm^{-1}, and 1734 cm^{-1}, which belong to the C═O absorption peaks, indicating the presence of the amide bond in CNH. Fig. 4a shows the powder X-ray diffraction (XRD) results, showing the four main peaks of CNH including 11.4°, 12.8°, 24° and 27.4°, which correspond to the main characteristic peaks of CN and hemin, respectively. The slight small angle offset of peak 27.4° compared to that of CN (27.6°) may have probably resulted from the insertion of the hemin molecule that might have broadened the interlamellar spacing of

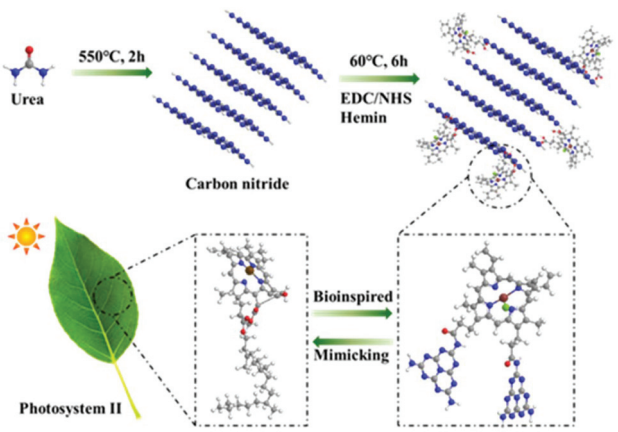

Fig. 3 Schematic representation of the CNH photocatalyst. The typical atom color description: dark brown (magnesium), brown (iron), green (chlorine), red (oxygen), blue (nitrogen), dark grey (carbon), and light grey (hydrogen).

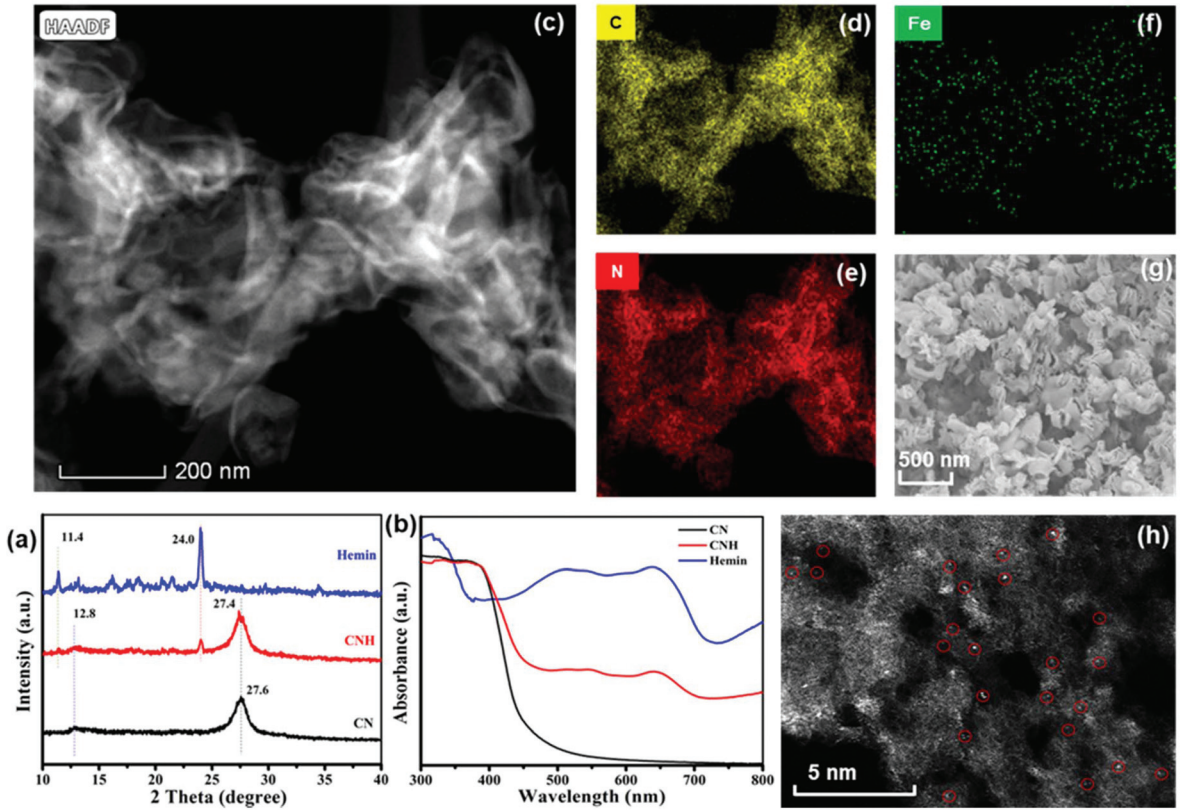

Fig. 4 Characterization of CNH. (a) XRD patterns; (b) UV spectra; (c) HAADF-STEM images with EDS mapping of (d) C, (e) N, and (f) Fe elements distributed in the same region; (g) SEM images; and (h) aberration-corrected high-resolution electron microscopy images.

CN. Moreover, the UV spectra indicate that CNH can combine the absorption wavelengths of CN and hemin, which can present an excellent absorption range for visible light (Fig. 4b). The BET analysis results show that the specific surface area of the CNH photocatalyst can remain unchanged when compared with that of CN (Fig. S1b†). But the pore diameter of CNH decreases from 2.0 to 10 nm, suggesting that the hemin molecules may fill into the bigger pores, making them smaller, as shown in Fig. S1c.† These comparative characterization results indicate that CN and hemin could be successfully cross-linked to yield CNH composites. Moreover, the morphology of CNH photocatalysts was characterized by HAADF-STEM imaging, showing a representative petal-like morphology (Fig. 4c). Also, the petal-like structures of CNH were further revealed by SEM imaging (Fig. 4g). Afterwards, the energy-dispersive X-ray spectroscopy (EDS) mapping was carried out for CNH, confirming the homogeneous distribution of C, N and Fe elements in the same region (Fig. 4d–f). Furthermore, the inductively coupled plasma mass spectrometry (ICP-MS) was conducted for the quantitative determination of single-atom iron site in the photocatalysts of CNH, and the results are given in Table S1.† Note that a loading of 0.646 mmol g^{-1} of iron over the petal-like CNH was determined by ICP-MS. More importantly, in the aberration-corrected image with atomic resolution (Fig. 4h), the bright spots with sizes of ~0.20 nm can correspond to the atomic dispersion of Fe sites on CNH. Therefore, the above results confirm that the petal-like biomimetic photocatalyst of CNH with excellent visible light absorption range has been successfully prepared by simple chemical cross-linking of CN with hemin under mild conditions, in which iron is uniformly distributed in a single atomic form.

Band structure and charge carrier behavior

The band structure can be seen in Fig. 5a–c. Based on the UV-vis absorption spectra shown in the figure, the bandgap energies of CN and hemin could be derived approximately by the Kubelka–Munk function *versus* photon energy (Fig. 5a and b). CN shows a suitable bandgap of 2.86 eV for visible light absorption, and a relatively narrow bandgap (1.28 eV) of hemin suggests the enhanced near-infrared light absorption. The flat band potential of CN, CNH and hemin is reflected by the Mott–Schottky plots, as shown in Fig. 5c. Obviously, the incorporation of hemin can make a negative offset of the Fermi level in CNH, as well as the conduction band (CB). Generally, the position of the CB is more negative than that of the Fermi level at 0.2 eV. Thus, the position of the CB in CN can be calculated at −1.37 eV, while the lowest unoccupied molecular orbital (LUMO) of hemin is −2.44 eV. In terms of the bandgaps in Fig. 5a and b, the valence band (VB) of CN and the highest occupied molecular orbital (HOMO) of hemin could be determined at 1.49 eV and −1.19 eV. Hence, the band structure of CNH could be confirmed logically. This energy-

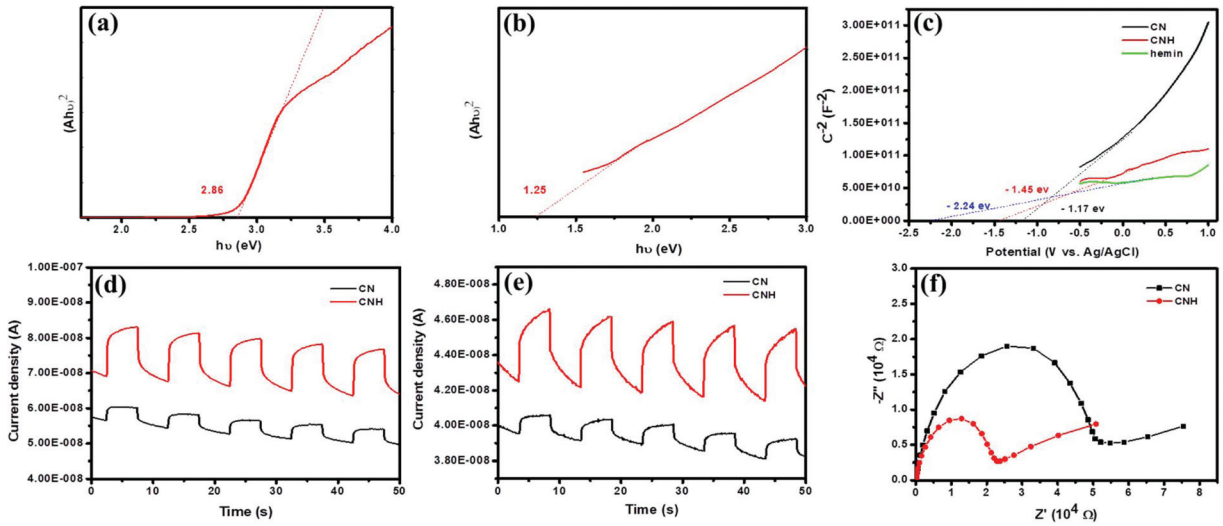

Fig. 5 (a) Band gap energy of CN. (b) Band gap energy of hemin. (c) Mott–Schottky plots (1000 Hz). (d) Transient photocurrent responses under visible light irradiation. (e) Transient photocurrent responses under red light (660 nm) irradiation. (f) The EIS Nyquist plots of CN and CNH.

level crossing effect contributes to the separation of photogenerated electron–hole pairs, leading to efficient reaction dynamics. Besides, the photoelectrochemical analysis showed the charge carrier behaviour in a typical three-electrode cell. Fig. 5d and e show the periodic on/off photocurrent responses of the catalysts under visible light and red light (660 nm) irradiation. CNH shows an approximate threefold increase in the photocurrent density, especially the enhanced responses to 660 nm compared with CN, indicating less recombination photogenerated carriers and improved utilization of near-infrared light.

Moreover, electrochemical impedance spectroscopy (EIS) was conducted in the dark to investigate the electronic conductivity (Fig. 5f); the semicircular Nyquist plot for CNH shows a minimum radius, indicating the lowest electron-transfer resistance. Therefore, CNH possesses a unique energy band structure and light absorption for the photogeneration of carriers with high reactivity to drive photocatalytic reactions efficiently.

Investigation of photocatalytic performances

To explore the performances of the developed biomimetic photocatalyst, the visible light-promoted sulfonation of alkenes with sulfinic acid was carried out in air at room temperature, aiming to obtain a highly bioactive drug block β-ketosulfone. Initially, styrene (**1a**) and *p*-methylbenzenesulfinic acid (**2b**) were chosen as model substrates to optimize the key reaction conditions, and the results are summarized in Table 1. Upon optimizing the key reaction parameters, the best results were obtained by performing the visible light-induced biomimetic catalysis with monoatomic site Fe-CNH at room temperature in an acidic environment in CH_3CN solvent, and the desired product **3ab** was obtained in 94% yield (Table 1, entry 1). Accordingly, the control experiments demonstrate that the catalyst, light, and the stoichiometric amount of acids during the sulfonation of alkenes should be the key factors responsible for the reaction yields (Table 1, entries 2–4). Moreover, the optimum concentration of the photocatalyst was observed to be 0.625 mg mL^{-1} (Table 1, entries 5 and 6). Nevertheless, to investigate the active sites of

Table 1 Optimization of the reaction conditions[a]

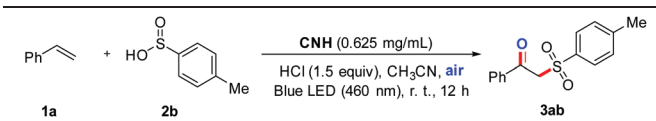

1a 2b 3ab

Entry	Deviation from standard conditions	Yield[b] (%)
1	None	94 (2861)
2	Without CNH	N. D.
3	Without light	27
4	Without HCl	62
5	1.25 mg mL^{-1} instead of 0.625 mg mL^{-1}	95
6	0.3125 mg mL^{-1} instead of 0.625 mg mL^{-1}	79
7	Hemin instead of CNH	65 (32)
8	CN instead of CNH	Trace
9	Hemin instead of CNH	24[c]
10	N_2 instead of air	Trace
11	Red LED: 630 nm	63

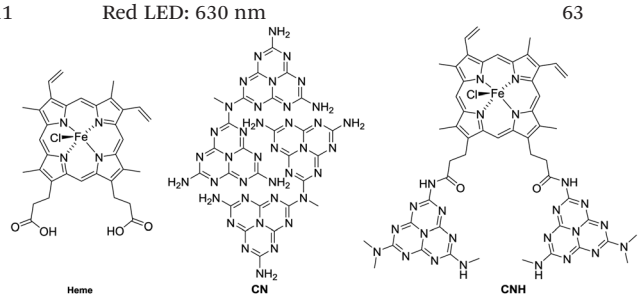

[a] Standard conditions: **1a** (0.5 mmol), **2b** (1.0 mmol), HCl (1.5 equiv.), CH_3CN (2.0 mL), air, blue LED (460 nm), r. t., and 12 h. "N.D." = not detected. [b] Isolated yield (TON). [c] Dark.

the CNH photocatalyst, hemin and CN were separately used to catalyze the standard reactions, and the products were obtained in 65% yields and trace amounts, respectively (Table 1, entries 7 and 8). Besides, a 24% yield was obtained under dark conditions when CNH was replaced by hemin (Table 1, entry 9). This indicates that Fe^{3+} ions show weak ability to oxidize sulfinic acid under air conditions to generate a sulfone radical to participate in the reaction *via* a different pathway.[11e] The turnover number (TON) of the prepared photocatalyst CNH (2861) was nearly ten times higher than that of CN (32), indicating that the introduction of CN can enhance the catalytic activity and stability of the photocatalyst CNH. Alternatively, after replacing the ambient conditions with nitrogen atmosphere, only trace amounts of the products could be obtained, indicating that air can also play a crucial role in the CNH photocatalytic reactions (Table 1, entry 10). Besides, the desired products could be obtained in moderate to good yields when the LED (460 nm) lamp was replaced by red light (630 nm) under the standard reaction conditions. It should be noted that it is otherwise impossible to achieve these products by the conventional photocatalytic reactions of organic synthesis (Table 1, entry 11).

To test the reusability of this biomimetic photocatalyst of the monoatomic Fe-containing CNH, repeated experiments were carried out using the same catalysts under the standard reaction conditions, except for using a new batch of reactants during each cycle. As seen from Fig. 6, a slight decrease in catalytic activity (to 85%) could be observed after five cycles of photocatalytic reactions. The reason for this decline might be the loss of the catalyst content during the centrifugal recovery process. Yet, the overall activities of the photocatalyst may still remain considerably high. These results convincingly confirm that the present protocol can serve as an efficient and recyclable heterogeneous photocatalysis strategy to synthesize β-ketosulfones with desirably high catalysis efficiencies.

Substrate scope

With the optimized conditions in hand, the scope and limitations of the CNH photocatalytic reactions of various alkene (**1**) substrates were explored using *p*-methylbenzenesulfinic acid (**2b**) to yield β-ketosulfones (**3**). The results are summarized in Table 2. It should be noted that a variety of alkenes containing electron-donating or electro-withdrawing substituents on the aryl groups are more suitable for the present protocol (**3ab–3gb**). In particular, various substituent functional groups such as F, Cl, Br, and CF_3 are more compatible with this protocol to access corresponding products (**3db–3gb**), which may be further functionalized to synthesize other kinds of complex molecules of great importance. Moreover, when the hydrogen at the *o*- or *m*-position of the benzene ring was substituted by chlorine, the activation reactions were not negatively affected (**3hb–3ib**). To our delight, altering the terminal olefins with the internal or cyclic olefins could also give the desired products in moderate yields (**3jb–3mb**). Besides, it was witnessed that the hydroxylated products could be readily obtained in excellent yields by replacing the terminal olefin with a six-membered cyclic alkene under the established conditions (**3lb–3mb**). Accordingly, the hydroxylated products should be the intermediates of the sulfonation reactions. It is noteworthy that the desired product **3nb** can be obtained in a moderate yield, when 2-vinylthiophene was used under the standard conditions. Unexpectedly, *N*-heterocycloolefin was highly selective to give the protonated product **3ob**, without the formation of β-ketosulfone. Unfortunately, the desired product **3pb** was not obtained when ester olefin was subjected to standard conditions.

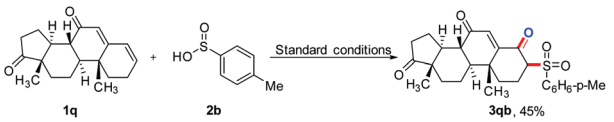

(1)

Meanwhile, the established protocol can be applied to the sulfonation reactions of androstenones to obtain the desired

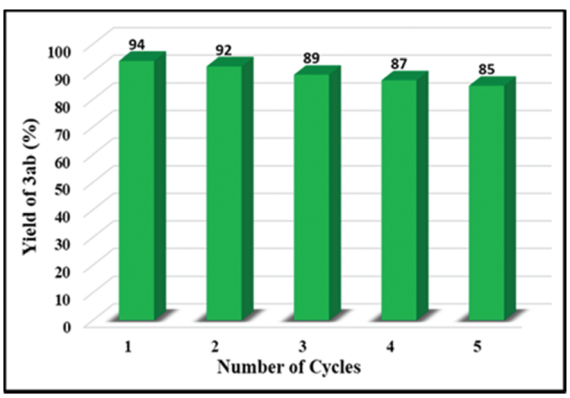

Fig. 6 Recycling experiments.

Table 2 Scope of alkenes[a,b]

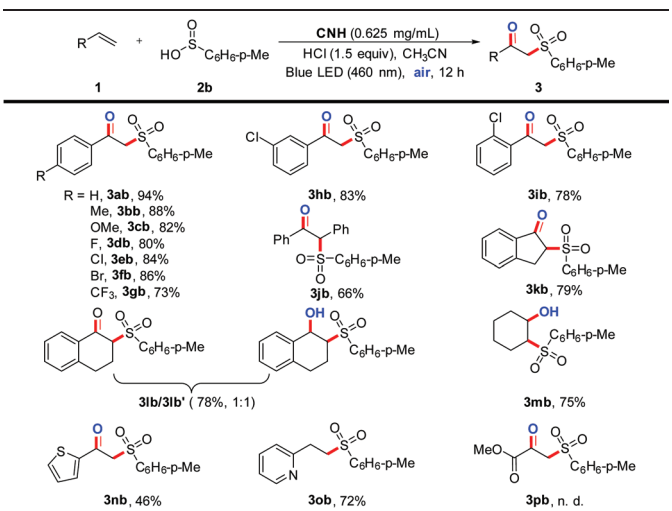

[a] Reaction conditions: **1** (0.25 mmol), **2b** (0.75 mmol), HCl (1.5 equiv.), CH_3CN (2.0 mL), air, blue LED (460 nm), r. t., and 12 h. [b] Isolated yields.

products in a yield of 45% (eqn (1)). The above results indicate that under the established reaction conditions, the developed biomimetic photocatalysis-based synthesis route can not only be suitably applied to the simple terminal aromatic olefins, but also to other types of olefins, such as internal alkenes, alkyl olefins, and macromolecular androstenediones.

Afterwards, as shown in Table 3, the investigation of different arylsulfinic acids suggests that all of the substrates bearing electron-rich and electron-deficient groups can be suitable for this photocatalytic reaction protocol to give the corresponding products in good yields (**3aa–3af**). More interestingly, the polysubstituted aromatic sulfinic acid and naphthalene-2-sulfinic acid could be tolerated under the model reaction conditions to give the desired products **3ag** and **3ah** in 78% and 84% yields, respectively. Additionally, alkyl sulfonates, such as sodium ethylsulfinate and sodium methylsulfinate, can also be obtained under the model reaction conditions in excellent yields (**3ai–3aj**).

Mechanistic studies

To gain further insights into the biomimetic-catalysed oxidative coupling mechanism of alkenes with sulfinic acids to form β-ketosulfones, a series of control experiments including electrochemical investigations by cyclic voltammetry (CV) were carried out using the photocatalyst CNH containing the monoatomic iron site (Scheme 1). Firstly, the active species trapping experiments were conducted to clarify the contribution of different active species in the reactions. Accordingly, ammonium oxalate (AO), benzoquinone (BQ) and sodium azide (NaN_3), which are the scavengers for hole, superoxide radical ($O_2^{\bullet-}$), and singlet oxygen ($^1O_2$), respectively, were selected to identify the active species.[13] It was found that the yields of the desired products could drastically decrease after separately adding AO, BQ, and NaN_3 under the standard conditions (Scheme 1a). Also, several similar experiments were carried out by replacing CNH with hemin under the standard conditions (Scheme 1b). The results show that hemin can generate the reactive oxygen species under visible light irradiation, which is not conducive to the separation of photo-

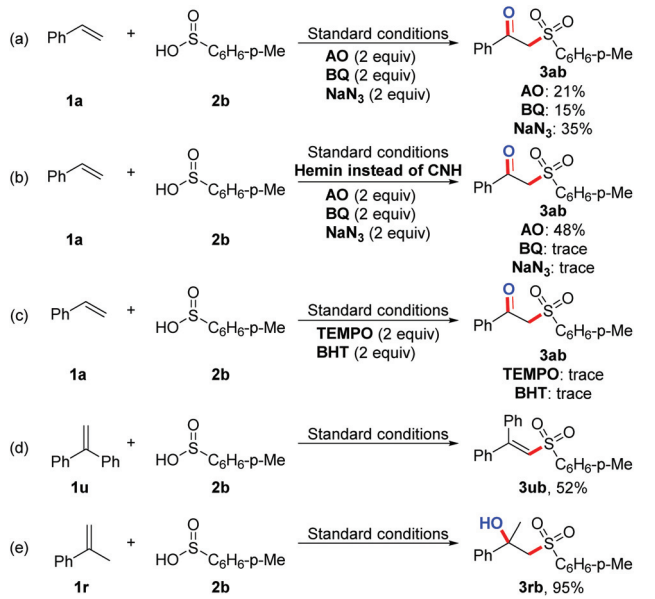

Scheme 1 Mechanism studies. (a), (b) Active species trapping experiments. (c) Radical inhibition experiments. (d) Radical trapping experiments. (e) The intermediate experiments.

generated electron–hole pairs. Hence, the singlet oxygen and superoxide radicals were determined as the major reactive species for the sulfonation of alkenes, and the introduction of CN can enhance the separation of photogenerated electron–hole pairs, which is more conducive to the progress of the reaction. Furthermore, it was discovered that the sulfonation reaction was inhibited when 2,2,6,6-tetramethyl-1-piperidinyloxy (TEMPO) or 2,6-di-tertbutyl-4-hydroxytoluene (BHT) was added into the present reaction system, suggesting that the reaction has presumably adopted a radical pathway (Scheme 1c). Moreover, the desired product **3ub** could be obtained in a yield of 52% when styrene was replaced with 1,1-diphenylethylene under the standard conditions, indicating the presence of a sulfone radical during the reaction process (Scheme 1d and Fig. S2†). Additionally, the desired product 2-phenyl-1-tosylpropan-2-ol **3rb** was obtained in 95% yield, when the reaction of prop-1-en-2-ylbenzene **1r** with 4-methylbenzenesulfinic acid **2b** proceeded under the standard conditions (Scheme 1e), which demonstrated that the hydroxylated products should be the intermediates of the sulfonation reactions. Finally, the electrochemical CV experiments were carried out to study the redox potentials of the substrates (Fig. S3†). An oxidation peak of **1a** in acetonitrile was observed at 0.82 V (*vs.* Ag/AgCl in acetonitrile), whereas the oxidation peak of **2a** was not observed. Therefore, it is thought that **1a** might be more easily oxidized than **2a** by the holes in the valence band (1.15 V *vs.* Ag/AgCl) under the standard reaction conditions.

Based on the above investigations and previous reports,[11a–c,e–g,14] a possible reaction mechanism (styrene and benzenesulfinic acid as models) is thereby proposed, as shown in Scheme 2. Initially, under visible light irradiation, the photocatalyst CNH has a stronger ability to separate

Table 3 Scope of sulfinic acids[a,b]

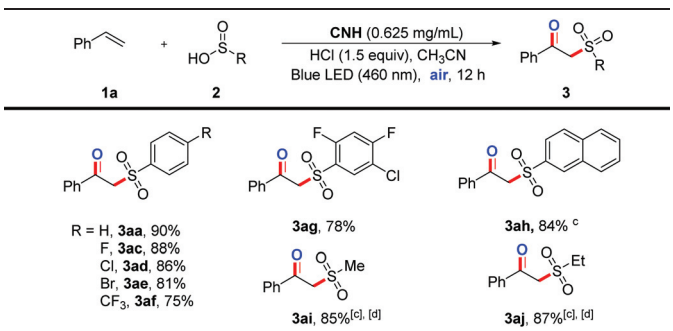

[a] Reaction conditions: **1a** (0.25 mmol), **2** (0.75 mmol), HCl (1.5 equiv.), CH_3CN (2.0 mL), air, blue LED (460 nm), r. t., and 12 h. [b] Isolated yields. [c] DMF instead of CH_3CN. [d] Sodium sulfinate.

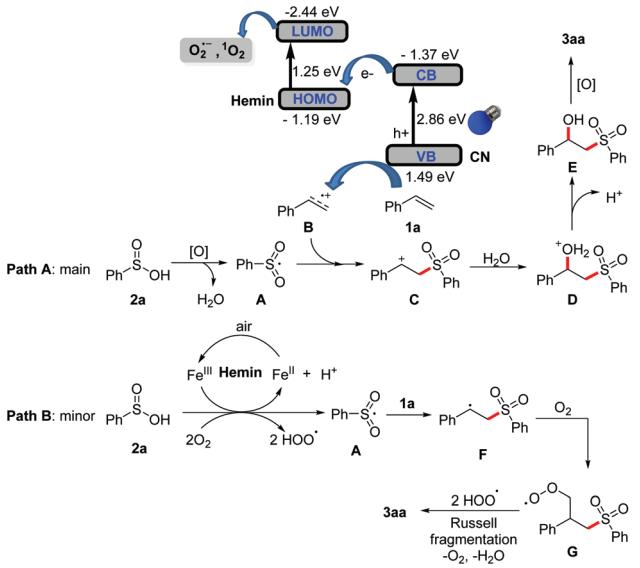

Scheme 2 Postulated reaction pathway.

photogenerated electron pairs and holes after cross-linking to composite hemin and CN. The photogenerated electrons would reduce molecular oxygen to produce $O_2^{\bullet-}$ and singlet oxygen $^1O_2$ by the lowest unoccupied molecular orbital of hemin. Furthermore, styrene **1a** can be oxidized to its radical cation **B** by the holes in the valence state of CN. Then, the obtained active oxygen species can oxidize benzenesulfinic acid **2a** to form sulfone radical **A**. Subsequently, the carbocation intermediate **C** is obtained by the cross-coupling of radical **A** and radical cation **B**. Finally, the nucleophilic attack of H_2O on the carbocation intermediate can produce intermediate **E**, which would be transformed into the desired product **3aa** under the oxidative conditions (path A, main). In addition, the sulfonyl radical **A** could also be produced *via* the single electron transfer (SET) and deprotonation process in the presence of hemin (Fe^{3+}) and dioxgyen.[11e] Subsequently, the addition of sulfonyl radical to alkene **1a** gives alkyl radical **F**, which is captured by dioxygen to generate peroxy radical **G**. Then, peroxy radical **G** interacted with $^{\bullet}OOH$ to form monoalkyl tetroxide intermediate and decomposed into the desired product **3aa** (path B, minor). Further investigation on the more detailed mechanism is ongoing in our laboratory.

Conclusions

In conclusion, we have successfully developed a facile and efficient protocol for the fabrication of a biomimetic photocatalyst with single-atom iron site by adopting a simple chemical cross-linked route. The as-prepared CNH was discovered to show the superior heterogeneous photocatalytic activity and high environmental stability for the sulfonation of olefins to access β-ketosulfones at atmospheric pressure and room temperature under visible and/or near-infrared light irradiation. Under the established reaction conditions, a series of new drug candidate products could be produced in good to high yields, together with excellent tolerance of functional groups. Particularly, this biomimetic photocatalytic aerobic oxidation strategy can be extensively applied to the sulfonation of androstenones with moderate to good yields. More importantly, this design concept of the present work provides wide opportunities for the development of the potential biomimetic catalytic systems with single-atom-site catalysts by using the cheap and green metal porphyrins or phthalocyanines. Further mechanism investigation and more practical application studies of this biomimetic photocatalysis-based synthesis method are currently underway in our laboratory.

Conflicts of interest

There are no conflicts to declare.

Acknowledgements

This work is supported by the National Natural Science Foundation of China (No. 21902083 and 21675099) and the Major Basic Research Program of the Natural Science Foundation of Shandong Province (ZR2018ZC0129), Shandong, P. R. China. This work is financially supported by the Southern University of Science and Technology (SUSTech) start fund through Shenzhen Peacock Talent Program, Guangdong Innovative and Entrepreneurial Research Team Program (No. 2016ZT06N532) and Guangdong Provincial Key Laboratory of Materials for Electric Power (2018B030322001) and special fund from Shenzhen Clean Energy Research Institute. This work is also supported by the Pico Center at SUSTech that received support from the Presidential fund and Development and Reform Commission of Shenzhen Municipality.

References

1 (*a*) D. Ravelli and M. Fagnoni, *ChemCatChem*, 2012, **4**, 169–171; (*b*) J. Xuan and W. J. Xiao, *Angew. Chem., Int. Ed.*, 2012, **51**, 6828–6838; (*c*) M. Parasram and V. Gevorgyan, *Chem. Soc. Rev.*, 2017, **46**, 6227–6240; (*d*) H. Yi, G. Zhang, H. Wang, Z. Huang, J. Wang, A. K. Singh and A. Lei, *Chem. Rev.*, 2017, **117**, 9016–9085; (*e*) S. Tang, L. Zeng and A. Lei, *J. Am. Chem. Soc.*, 2018, **140**, 13128–13135; (*f*) Q. Q. Zhou, Y. Q. Zou, L. Q. Lu and W. J. Xiao, *Angew. Chem., Int. Ed.*, 2019, **58**, 1586–1604.

2 (*a*) M. Cherevatskaya, M. Neumann, S. Füldner, C. Harlander, S. Kümmel, S. Dankesreiter, A. Pfitzner, K. Zeitler and B. König, *Angew. Chem., Int. Ed.*, 2012, **51**, 4062–4066; (*b*) X. Lang, X. Chen and J. Zhao, *Chem. Soc. Rev.*, 2014, **43**, 473–486; (*c*) J. Chen, J. Cen, X. Xu and X. Li, *Catal. Sci. Technol.*, 2016, **6**, 349–362; (*d*) Y. Cai, Y. Tang, L. Fan, Q. Lefebvre, H. Hou and M. Rueping, *ACS Catal.*, 2018, **8**, 9471–9476; (*e*) A. Savateev, I. Ghosh, B. König and

M. Antonietti, *Angew. Chem., Int. Ed.*, 2018, **57**, 15936–15947; (*f*) Q. Gu, Q. Jia, J. Long and Z. Gao, *ChemCatChem*, 2019, **11**, 669–683; (*g*) B. Kurpil, K. Otte, A. Mishchenko, P. Lamagni, W. Lipiński, N. Lock, M. Antonietti and A. Savateev, *Nat. Commun.*, 2019, **10**, 945; (*h*) X. Zhu, Y. Lin, J. S. Martin, Y. Sun, D. Zhu and Y. Yan, *Nat. Commun.*, 2019, **10**, 2843.

3 (*a*) J. Zoller, D. C. Fabry and M. Rueping, *ACS Catal.*, 2015, **5**, 3900–3904; (*b*) I. Ghosh, J. Khamrai, A. Savateev, N. Shlapakov, M. Antonietti and B. König, *Science*, 2019, **365**, 360–366.

4 (*a*) M. Mousavi, A. Habibi-Yangjeh and S. R. Pouran, *J. Mater. Sci.: Mater. Electron.*, 2018, **29**, 1719–1747; (*b*) P. Rana, R. Gaur, R. Gupta, G. Arora, J. Anireddy and R. K. Sharma, *Chem. Commun.*, 2019, **55**, 7402–7405.

5 (*a*) J. Long, S. Wang, Z. Ding, S. Wang, Y. Zhou, L. Huang and X. Wang, *Chem. Commun.*, 2012, **48**, 11656–11658; (*b*) K. G. Laurier, F. Vermoortele, R. Ameloot, D. E. De Vos, J. Hofkens and M. B. Roeffaers, *J. Am. Chem. Soc.*, 2013, **135**, 14488–14491; (*c*) X. Deng, Z. Li and H. García, *Chem. – Eur. J.*, 2017, **23**, 11189–11209.

6 Y. Zhi, Z. Li, X. Feng, H. Xia, Y. Zhang, Z. Shi, Y. Mu and X. Liu, *J. Mater. Chem. A*, 2017, **5**, 22933–22938.

7 (*a*) L. Moehlmann, M. Baar, J. Riess, M. Antonietti, X. Wang and S. Blechert, *Adv. Synth. Catal.*, 2012, **354**, 1909–1913; (*b*) B. Kurpil, Y. Markushyna and A. Savateev, *ACS Catal.*, 2019, **9**, 1531–1538.

8 (*a*) M. Rueping, J. Zoller, D. C. Fabry, K. Poscharny, R. M. Koenigs, T. E. Weirich and J. Mayer, *Chem. – Eur. J.*, 2012, **18**, 3478–3481; (*b*) H. E. Ho, Y. Ishikawa, N. Asao, Y. Yamamoto and T. Jin, *Chem. Commun.*, 2015, **51**, 12764–12767.

9 H. Wei, X. Liu, A. Wang, L. Zhang, B. Qiao, X. Yang, Y. Huang, S. Miao, J. Liu and T. Zhang, *Nat. Commun.*, 2014, **5**, 5634.

10 (*a*) P. A. Bartlett, F. R. Green III and E. H. Rose, *J. Am. Chem. Soc.*, 1978, **100**, 4852–4858; (*b*) R. E. Swenson, T. J. Sowin and H. Q. Zhang, *J. Org. Chem.*, 2002, **67**, 9182–9185; (*c*) H. Yang, R. G. Carter and L. N. Zakharov, *J. Am. Chem. Soc.*, 2008, **130**, 9238–9239; (*d*) Y. M. Markitanov, V. M. Timoshenko and Y. G. Shermolovich, *J. Sulfur Chem.*, 2014, **35**, 188–236; (*e*) S. Trivedi, P. C. Patidar, P. K. Chaurasiya, R. S. Pawar, U. K. Patil and P. K. Singour, *Pharma Chem.*, 2010, **2**(4), 369–377; (*f*) W. M. Wolf, *J. Mol. Struct.*, 1999, **474**, I13–124; (*g*) J. Xiang, M. Ipek, V. Suri, W. Massefski, N. Pan, Y. Ge, M. Tam, Y. Xing, J. F. Tobin, X. Xu and S. Tam, *Bioorg. Med. Chem. Lett.*, 2005, **15**, 2865–2869; (*h*) H. O. House and J. K. Larson, *J. Org. Chem.*, 1968, **33**, 61–65.

11 (*a*) Q. Lu, J. Zhang, G. Zhao, Y. Qi, H. Wang and A. Lei, *J. Am. Chem. Soc.*, 2013, **135**, 11481–11484; (*b*) W. Wei, C. Liu, D. Yang, J. Wen, J. You, Y. Suo and H. Wang, *Chem. Commun.*, 2013, **49**, 10239–10241; (*c*) A. K. Singh, R. Chawla, T. Keshari, V. K. Yadav and L. D. S. Yadav, *Org. Biomol. Chem.*, 2014, **12**, 8550–8554; (*d*) X. Tang, L. Huang, Y. Xu, J. Yang, W. Wu and H. Jiang, *Angew. Chem., Int. Ed.*, 2014, **53**, 4205–4208; (*e*) W. Wei, J. Wen, D. Yang, M. Wu, J. You and H. Wang, *Org. Biomol. Chem.*, 2014, **12**, 7678–7681; (*f*) V. K. Yadav, V. P. Srivastava and L. D. S. Yadav, *Synlett*, 2016, **27**, 427–431; (*g*) D. Yang, B. Huang, W. Wei, J. Li, G. Lin, Y. Liu, J. Ding, P. Sun and H. Wang, *Green Chem.*, 2016, **18**, 5630–5634.

12 (*a*) D. Mansuy, *Pure Appl. Chem.*, 1990, **62**, 741–746; (*b*) R. A. Sheldon, *Metalloporphyrins in catalytic oxidations*, CRC Press, 1994; (*c*) W.-J. Yang and C.-C. Guo, *Chin. J. Appl. Chem.*, 2004, **21**, 541–545; (*d*) M. Costas, *Coord. Chem. Rev.*, 2011, **255**, 2912–2932; (*e*) Q. Liu and C. Guo, *Sci. China: Chem.*, 2012, **55**, 2036–2053; (*f*) M. M. Pereira, L. D. Dias and M. J. Calvete, *ACS Catal.*, 2018, **8**, 10784–10808; (*g*) R. Singh and A. Mukherjee, *ACS Catal.*, 2019, **9**, 3604–3617.

13 Y. Xiao, G. Tian, W. Li, Y. Xie, B. Jiang, C. Tian, D. Zhao and H. Fu, *J. Am. Chem. Soc.*, 2019, **141**, 2508–2515.

14 (*a*) M. Nishikimi, *Biochem. Biophys. Res. Commun.*, 1975, **63**, 463–468; (*b*) J. Cadet and R. Teoule, *Photochem. Photobiol.*, 1978, **28**, 661–665; (*c*) C. Bolm, J. Legros, J. Le Paih and L. Zani, *Chem. Rev.*, 2004, **104**, 6217–6254; (*d*) E. Floriano-Sánchez, C. Villanueva, N. Medina-Campos and D. Rocha, *Free Radical Res.*, 2006, **40**, 523–533.